Terahertz carpet cloak based on a ring resonator metasurface

B. Orazbayev,[1,*] N. Mohammadi Estakhri,[2] M. Beruete,[1] and A. Alù[2]
[1]*Antennas Group-TERALAB, Universidad Pública de Navarra, Campus Arrosadía, 31006 Pamplona, Spain*
[2]*Department of Electrical and Computer Engineering, The University of Texas at Austin, Austin, Texas 78712, USA*
(Received 18 March 2015; revised manuscript received 7 May 2015; published 29 May 2015)

In this work we present the concept and design of an ultrathin ($\lambda/22$) terahertz (THz) unidirectional carpet cloak based on the local phase compensation approach enabled by gradient metasurfaces. A triangular surface bump with center height of 4.1 mm (1.1λ) and tilt angle of 20° is covered with a metasurface composed of an array of suitably designed closed ring resonators with a transverse gradient of surface impedance. The ring resonators provide a wide range of control for the reflection phase with small absorption losses, enabling efficient phase manipulation along the edge of the bump. Our numerical results demonstrate a good performance of the designed cloak in both near field and far field, and the cloaked object mimics a flat ground plane within a broad range of incidence angles, over 35° angular spectrum centered at 45°. The presented cloak design can be applied in radar and antenna systems as a thin, lightweight, and easy to fabricate solution for radio and THz frequencies.

DOI: 10.1103/PhysRevB.91.195444 PACS number(s): 42.25.Fx, 41.20.Jb, 78.67.Pt

I. INTRODUCTION

Metamaterials have opened new directions to tailor at will the intrinsic electromagnetic parameters of a composite, such as its permittivity and permeability, providing interesting solutions for one of the oldest quests of electromagnetism—controlling electromagnetic waves at will [1,2]. Many devices have been proposed based on metamaterials, ranging from lenses [3,4] and beam steering structures [5] to cloaking devices [6–9] able to hide objects from an external observer. After years of intensive studies, several cloaking mechanisms and designs have been proposed, mostly among the two leading categories of transformation optics [10,11] and scattering cancellation [12–14]. The techniques based on transformation optics impose strong demands on bulk metamaterial designs, such as a specific profile of inhomogeneity and anisotropy of the material parameters. These constraints make such cloaking devices difficult to realize in practice, due to their high complexity. The scattering cancellation cloaks are simpler to realize and more robust [15], yet, like any passive cloaking technique, they suffer from fundamental limitations on the size of the object to be cloaked [16].

A cloaking approach that relaxes the causality limitations on size and bandwidth is known as carpet cloaking or ground cloaking, with the idea of hiding in reflection a bump on a mirror. This problem has gained the interest of many researchers, due to its inherently relaxed constraints, its simplified design, and wide range of applications. Transformation-based carpet cloaks exploit quasiconformal mapping [17,18], which allows to minimize the anisotropy of the required material and can be implemented using isotropic dielectrics [19], simplifying the design and minimizing absorption losses. However, the proposed cloak is still volumetric and non-trivial to realize. Another important hurdle for practical applications of carpet cloaks is the lateral shift they introduce under the isotropic approximation. Unfortunately, the introduced lateral shift is comparable to the case when a ground plane is placed above the cloaked object to suppress its scattering. Since the cloaking medium is typically denser than free space, the beam inside the cloak is refracted into a smaller angle. However, if we require that a finite-size beam emerges from the cloak at the same location as it would when reflected by a flat ground plane, it should be refracted into a larger angle, which is only possible in anisotropic materials. This lateral shift presents a serious problem, since an external observer still can notice that the beam emerges from a different point [20] and it also begs the question of whether another flat reflector on top of the bump would not provide a simpler solution to the problem.

To overcome the issues associated with conventional ground cloaking approaches, recently it has been proposed that covering a bump with a specially designed surface can reduce unwanted scattering from an arbitrary bump, creating an effective ultrathin cloaking surface [21,22]. The metasurface is used to build a phase distribution on the bump edge equal to the phase response created upon reflection from a conducting ground plane, i.e., when no bump is present. In this case, for the external observer the reflected wave will have the same phase distribution as if it were reflected from the ground plane, creating an ultrathin and relatively simple cloaking configuration for practical implementation. Moreover, due to surface phase compensation, the metasurface cloak does not create a lateral shift [21]. Obviously this approach is dependent on the object to be hidden and the illumination, but, given its robustness, it may provide a viable solution for several practical applications, as we discuss in the following.

In this work, we propose an ultrathin metasurface-based carpet cloak suitable for THz regime, we report successful concealment of an electrically large object in the near and far field, and we provide a thorough analysis of the angle and frequency dependence of the device performance. Our cloak is based on the concept originally introduced in Refs. [21,22] applied to a triangular bump with center height of 4.1 mm ($1.1\lambda_0$) at 80 GHz. However, in Ref. [21] the cloak is designed for a normal incidence with small range of the incident angles (∼5°). In contrast to the results in Ref. [22] we obtain the carpet cloak for an electrically large object—the height of the bump is 4.1 mm ($1.1\lambda_0$). We demonstrate a good performance within

*Corresponding author: b.orazbayev@unavarra.es

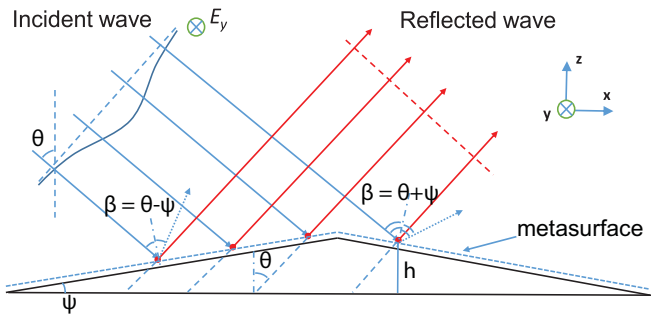

FIG. 1. (Color online) Scheme of the carpet cloak with metasurface.

35° range of the incidence angle and a frequency bandwidth of 8 GHz, with 10% fractional bandwidth (FBW).

II. CARPET CLOAK DESIGN

Figure 1 shows the general scheme of the cloak and of the object. The incoming oblique wave, with angle of incidence θ (with respect to the horizontal ground plane), illuminates a PEC bump with a tilt angle ψ. Any arbitrary object we aim to conceal can be placed inside the bump, as long as it fits in its volume. The goal is to create a field distribution on the external boundary of the object (dashed line), identical to the case when no bump is presented, in view of the field equivalence principle. This technique is different from carpet cloaks based on the quasiconformal mapping, where the object is concealed by controlling the propagation of the incident waves and effectively isolating the hidden region from the incident wave. Here, reconstruction of the field can be done by introducing an abrupt phase variation on the boundary, which can be calculated at each point of the bump's edge as Ref. [22]:

$$\delta = \pi - 2k_0 h \cos\theta \tag{1}$$

where k_0 is the free space wave vector at the operation frequency, h is the height of the unit cell center from the ground plane, and θ is the angle of incidence of the incoming wave with respect to the back-plane normal.

III. NUMERICAL RESULTS

A. Cloaking metasurface

In order to obtain the required phase distribution, a metasurface based on pairs of closed ring resonators (CRR) is used, whose unit cell is shown in the inset of Fig. 2(a). A clear advantage of such topology is its insensitivity to the polarization of the incident electromagnetic field. To realize the effect, we need to control the phase response of the reflected wave from each block over the entire 2π phase range. To this purpose, we simulated the reflection from infinite planar arrays of such closed rings using the commercial software CST Microwave Studio™ [23], using unit cell boundaries and frequency-domain solver. A fine tetrahedral mesh was chosen with maximum edge length 0.285 mm ($0.076\lambda_0$) and minimum edge length 0.0007 mm ($0.0002\lambda_0$). To create a high-resolution surface with better control over the phase distribution of the reflected beam, the lateral dimension

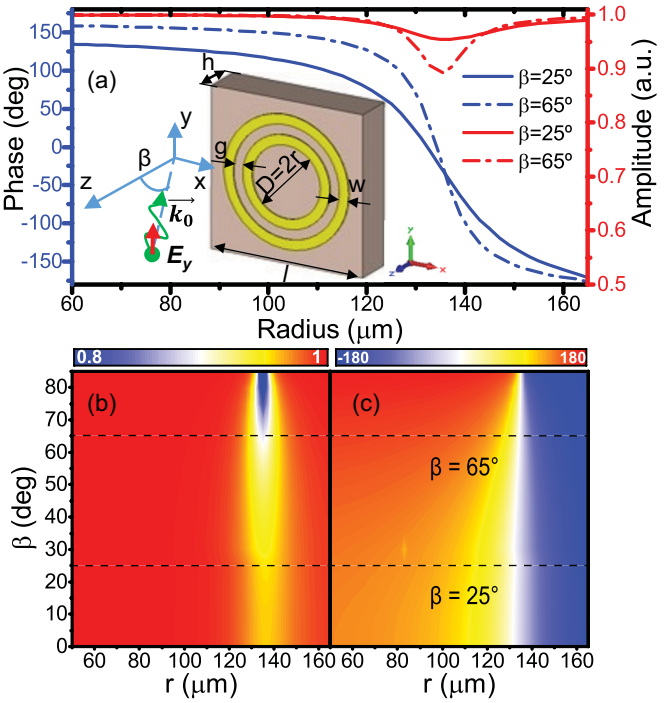

FIG. 2. (Color online) (a) Phase response of the unit cell for different angles of incidence. (Inset indicates the unit cell geometry and its corresponding parameters.) Color-map for the amplitude (b) and phase (c) of the reflection coefficient as a function of the incidence angle and radius of the inner ring.

of the unit cell was fixed at 400 μm $\approx \lambda_0/10$, for the working frequency $f = 80$ GHz ($\lambda_0 = 3.75$ mm). Each unit cell consists of two concentric metallic rings with a fixed width $w = 10$ μm, separated by a gap $g = 10$ μm. The radius of the outer ring is then found as $r_2 = r_1 + w + g$, where r_1 is the radius of the inner ring. The rings are separated from the ground plane by a thin silicon layer of thickness $h = 165$ μm ($\approx\lambda_0/22$) with dielectric permittivity $\varepsilon_r = 11.2$ and loss tangent $\tan\delta = 4.7 \times 10^{-6}$. The metal used for the rings is aluminum with a conductivity $\sigma_{Al} = 3.56 \times 10^7$ S/m.

Due to the geometry of the carpet cloak, the incoming wave has two possible incidence angles (β) on each block of the metasurface, depending on which side of the bump the block is located. In our particular case for an obliquely incident wave with angle $\theta = 45°$ and tilt angle of the bump $\psi = 20°$, the incidence angles at the bump edges are $\beta_1 = \theta - \psi = 25°$ and $\beta_2 = \theta + \psi = 65°$ for the left and right side, respectively. The amplitude and phase of the reflection coefficient was obtained as a function of radius of the inner ring and the angle of incidence β, shown in Figs. 2(b) and 2(c). In order to increase the design precision, instead of the normal reflection coefficients, here we design the cloaking layers on each side of the bump based on the data calculated for the corresponding incidence angles. As observed in Figs. 2(a) and 2(b), the amplitude of the reflected beam slightly drops around $r_1 = 135$ μm, due to the CRR resonance. Apart from the resonance, however, the metasurface is operating almost as an ideal mirror with close to unitary efficiency. Fig. 2(a) also shows the phase response of the unit cell for two incidence angles β_1 (solid blue line) and β_2 (dash dotted blue line). The range of phase

variation attainable by changing the inclusion radius spans almost 2π, confirming that this unit cell can adequately control the local phase response of the cloaking metasurface. It is also clearly seen that for a larger incidence angle the phase response has a steeper slope and, therefore, it is more sensitive to the radius variation of the rings, as it may be expected. This means that a bump with a larger tilt angle requires a metasurface with a smaller variation of radii, in the order of a few μm.

B. Final design

Once the phase response of the unit cell has been characterized, it is possible to put together the carpet cloak using the design equation (1), in order to hide a perfectly conducting bump with triangular shape lying in the xz plane and infinite in the transverse y direction. For practical realizations, it is preferred to cloak electrically large objects with bigger tilt angles, which allows us to more efficiently utilize the space under the cloak. Extreme shapes and large corner angles may require nonlocal and active surfaces [24], but for slowly varying configurations, including the current proposed design, surface phase engineering is adequate [21]. In this example, the ground cloak was designed for a bump with a tilt angle $\psi = 20°$, height of 4.1 mm ($1.1\lambda_0$), edge length of 12 mm ($3.2\lambda_0$) and base length 22.5 mm ($6\lambda_0$). Full-wave simulations of the structure were performed using the transient solver CST Microwave Studio^{TM}. The structure was illuminated by an obliquely incident ($\theta = 45°$) Gaussian beam with *TE* polarization. To this end, an array of electric dipoles was used with Gaussian distribution of amplitudes, providing a quasi-Gaussian beam excitation. The ground plane was emulated by using an electric boundary (perfect electric conductor) in the xy plane ($z = 0$). Given the symmetry of the structure, an electric symmetry was applied in the xz plane ($y = l/2$) in order to reduce computational time. A fine hexahedral mesh was applied with minimum cell length of 0.1 mm ($0.026\lambda_0$) and maximum of 0.44 mm ($0.112\lambda_0$)

As explained above, the phase response of the each block was obtained using unit cell boundaries, assuming that all cells in each simulation have the same parameters. On the contrary, to successfully mimic the ground plane, the radii of the rings must change according to the phase distribution determined by (1). The transverse inhomogeneities modify the mutual coupling between adjacent blocks and, therefore, its response to the incident wave. Hence, an optimization procedure is required to fine tune the design based on (1), imparting a local variation to the radii of surface blocks (60 blocks in the current design). Due to the reciprocity principle [25], we need to optimize only half of the bump, so only 30 unit cells need to be considered in the optimization process.

Figures 3(a)–3(c) show the spatial distribution of the electric field (E_y component) at the operation frequency $f_0 =$ 80 GHz for three cases: ground plane [(Fig. 3(a)], bare bump [Fig. 3(b)], and cloaked bump [Fig. 3(c)]. As it can be seen, when an irregularity is introduced on the ground plane the Gaussian beam is scattered over a wide range of angles. After the cloak is applied, the near-field distribution of the reflected wave is restored to the original Gaussian beam. The small disturbance of the reflected beam is caused by the finite discretization of the cloaking metasurface and high ($\beta = 65°$) incidence angle at the second edge of the bump, which may be mitigated with active cloaking surfaces [24]. As it was shown in Fig. 2(a) absorption losses are higher for high angles of incidence, provoking higher scattering level. Despite all these factors, Fig. 4 demonstrates that we are able to obtain a similar far-field radiation pattern from the cloaked beam as if a bare ground plane were interacting with the incident wave.

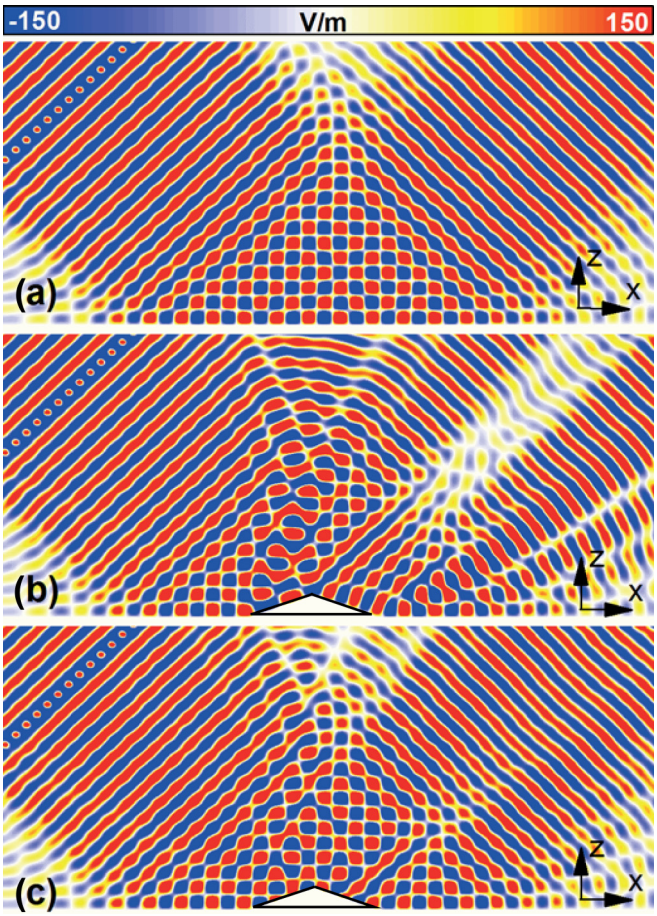

FIG. 3. (Color online) Electric field distribution on xz plane for (a) ground plane, (b) bare bump, and (c) cloaked bump.

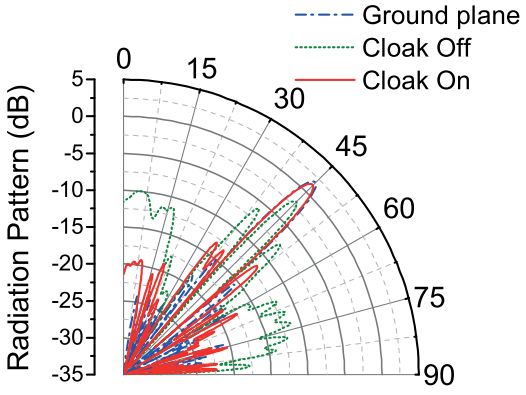

FIG. 4. (Color online) Radiation pattern for the reflected Gaussian beam from the ground plane (dash-dotted blue line), the bump without cloak (dotted green line), and from the cloaked bump (solid red line).

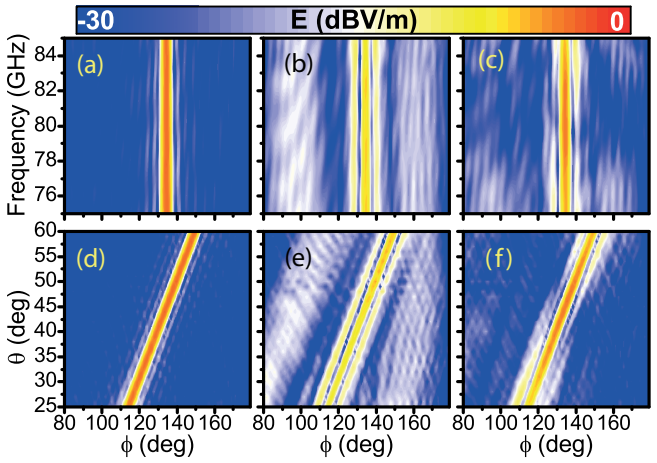

FIG. 5. (Color online) Amplitude of the far-field component of the electric field as a function of azimuth angle φ and frequency (a)–(c) and as a function of the incidence angle θ and azimuth angle φ (d)–(f). Left column refers to the beam reflected from the ground plane, center from the bare bump, and right column from the bump covered with the cloak.

C. Carpet cloak bandwidth

Next, the performance of the optimized cloak was analyzed in terms of the angle and frequency bandwidth. For this study, the numerical simulations were run within a frequency span from 75–85 GHz with a step of 0.2 GHz and steering the incidence angle from 25°–60° with a step of 1°. The resulting color maps for the far-field scattering electric field magnitude as a function of azimuth angle and frequency are shown in Figs. 5(a)–5(c). The analogous color maps for the far-field magnitude as a function of azimuth angle and incident angle θ of the incoming wave are shown in Figs. 5(d)–5(f). The cloak works close to ideally at the designed frequency and angle of incidence, yet, and in spite of the original unidirectional design, it is able to significantly reduce the scattering level in the whole simulated range of frequencies and incidence angles. The multilobe pattern created in the presence of the bump is converted into a directive beam, as desired for an ideal ground plane. In order to quantitatively define the region over which the beam reconstruction is acceptable we use a root mean square error (RMSE) function, which determines the goodness of the fit, and can be defined as [26]:

$$\mathrm{RMSE}(f,\theta) = \sqrt{\frac{1}{N}\sum_{i=1}^{N}[E_s(f,\theta,\varphi_i) - E_b(f,\theta,\varphi_i)]^2} \quad (2)$$

where N is the number of sample azimuth angles, $E_s(f,\theta,\varphi_i)$ and $E_b(f,\theta,\varphi_i)$ are the far-field magnitude of the reflected wave from the bump and the ground plane at given azimuth angle φ_i, frequency f, and incident angle θ. The calculated RMSE(f,θ) for the scattered beam without and with the cloak are shown in Figs. 6(a) and 6(b). A sufficiently accurate fit is considered for the RMSE less than 10% [27]. Hence, our parametric study reveals that the ground cloak maintains a reasonable performance in a frequency span of about 8 GHz (fractional bandwidth FBW = 10%) and angular span of 35°. In addition, it is noticeable that the cloak has a wider bandwidth for the lower incident angles, which is in good agreement with our previous study for the phase response as a function of the incident angle β. For applications in which the accuracy of the recovered beam is important, for example for high-precision measurements, an RMSE below 5% [dashed contour line in Fig. 6(b)] would still provide a bandwidth of 2.2 GHz (FBW = 3%) and angular span of 10°.

These results have been obtained for relatively small substrate losses ($\tan\delta = 4.7\times10^{-6}$ or $\sigma = 2.5\times10^{-4}$ S/m). However, in practical realizations the losses can be several orders higher and may disrupt the cloak operation. Therefore, an analysis of the performance of the cloak was done for higher values of dielectric losses. The recovery of the Gaussian beam at the operational frequency 80 GHz was estimated for different values of conductivity, using the same RMSE metric, and corresponding results are plotted in Fig. 6(c). Interestingly, even for very low RMSE (<5%) the cloaking metasurface is able to recover the far-field pattern of the original reflected Gaussian beam for values of conductivity up to 1.2 S/m ($\tan\delta = 0.023$), as it may be expected due to the inherently nonresonant nature of the proposed cloaking technique. Silicon samples with an equivalent value of resistivity $\rho = 83\,\Omega\,\mathrm{cm}$ are relatively cheap and commercially available, making the proposed cloaking device appealing for low-cost THz

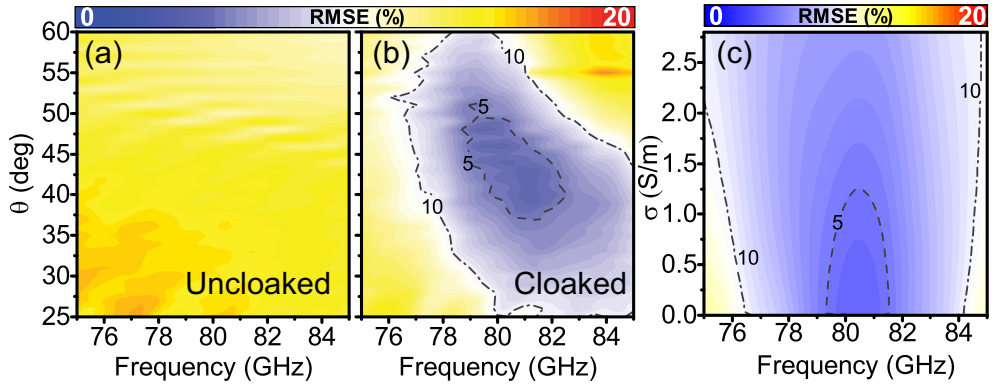

FIG. 6. (Color online) RMSE distribution vs incident angle and frequency for (a) uncloaked and (b) cloaked bump. (c) RMSE distribution as a function of the conductivity σ of dielectric substrate and frequency.

devices such as automotive radar systems, to reduce unwanted scattering from electrically large objects.

IV. CONCLUSIONS

To conclude, in this paper we have presented a thorough numerical study of an ultrathin ($\lambda/22$) carpet cloak based on a smartly engineered graded metasurface. The proposed cloaking metasurface is polarization insensitive and has a simple geometry, which facilitates the fabrication and reduces cost. Moreover, the proposed cloak demonstrates an acceptable beam reconstruction over a good angular span of 35° and a moderately broad bandwidth FBW = 10%. Such a cloak can conceal electrically large objects and may find applications in radar and antenna systems, where other techniques may be unpractical due to their excessively large volumes.

ACKNOWLEDGMENTS

This work was supported in part by the Spanish Government under Contract Consolider Engineering Metamaterials CSD2008-00066 and Contract TEC2011-28664-C02-01. B.O. is sponsored by the Spanish Ministerio de Economía y Competitividad under Grant No. FPI BES-2012-054909. M.B. is sponsored by the Spanish Government via RYC-2011-08221. N.M.E. and A.A. have been supported by the NSF CAREER Award No. ECCS-0953311 and the AFOSR Grant No. FA9550-13-1-0204.

[1] N. Engheta and R. W. Ziolkowski, *Metamaterials: Physics and Engineering Explorations* (Wiley, Hoboken, 2006).
[2] L. Solymar and E. Shamonina, *Waves in Metamaterials* (Oxford University Press, Oxford, 2009).
[3] J. B. Pendry, Phys. Rev. Lett. **85**, 3966 (2000).
[4] Z. Liu, H. Lee, Y. Xiong, C. Sun, and X. Zhang, Science **315**, 1686 (2007).
[5] V. Pacheco-Peña, V. Torres, B. Orazbayev, M. Beruete, M. Navarro-Cía, M. Sorolla Ayza, and N. Engheta, Appl. Phys. Lett. **105**, 243503 (2014).
[6] D. Schurig, J. J. Mock, B. J. Justice, S. A. Cummer, J. B. Pendry, A. F. Starr, and D. R. Smith, Science **314**, 977 (2006).
[7] M. Silveirinha, A. Alù, and N. Engheta, Phys. Rev. E **75**, 036603 (2007).
[8] D. Shin, Y. Urzhumov, Y. Jung, G. Kang, S. Baek, M. Choi, H. Park, K. Kim, and D. R. Smith, Nature Commun. **3**, 1213 (2012).
[9] N. Landy and D. R. Smith, Nature Mater. **12**, 25 (2013).
[10] U. Leonhardt, Science **312**, 1777 (2006).
[11] J. B. Pendry, D. Schurig, and D. R. Smith, Science **312**, 1780 (2006).
[12] A. Alù and N. Engheta, Phys. Rev. E **72**, 016623 (2005).
[13] A. Alù, M. G. Silveirinha, and N. Engheta, Phys. Rev. E **78**, 016604 (2008).
[14] D. Rainwater, A. Kerkhoff, K. Melin, J. C. Soric, G. Moreno, and A. Alù, New J. Phys. **14**, 013054 (2012).
[15] A. Alù and N. Engheta, Opt. Express **15**, 3318 (2007).
[16] F. Monticone and A. Alù, Phys. Rev. X **3**, 041005 (2013).
[17] J. Li and J. B. Pendry, Phys. Rev. Lett. **101**, 203901 (2008).
[18] R. Liu, C. Ji, J. J. Mock, J. Y. Chin, T. J. Cui, and D. R. Smith, Science **323**, 366 (2009).
[19] P. Zhang, M. Lobet, and S. He, Opt. Express **18**, 18158 (2010).
[20] B. Zhang, T. Chan, and B.-I. Wu, Phys. Rev. Lett. **104**, 233903 (2010).
[21] J. Zhang, Z. Lei Mei, W. Ru Zhang, F. Yang, and T. Jun Cui, Appl. Phys. Lett. **103**, 151115 (2013).
[22] N. M. Estakhri and A. Alu, IEEE Antennas Wirel. Propag. Lett. **13**, 1775 (2014).
[23] CST Computer Simulation Technology AG, www.cst.com, (2015).
[24] N. Mohammadi Estakhri, C. Argyropoulos, and A. Alù, Philos. Trans. R. Soc. London (to be published).
[25] D. L. Sounas and A. Alù, Opt. Lett. **39**, 4053 (2014).
[26] I. Moreno and C.-C. Sun, Opt. Express **16**, 1808 (2008).
[27] C. Daniel and F. S. Wood, *Fitting Equations to Data: Computer Analysis of Multifactor Data for Scientists and Engineers* (Wiley, New York, 1971).